Flow Turbulence Combust (2006) 77: 77–95
DOI 10.1007/s10494-006-9038-2

Use of Time Resolved PIV for Validating LES/DNS of the Turbulent Flow within a PCB Enclosure Model

G. Usera · A. Vernet · J. A. Ferré

Accepted: 12 January 2006 / Published online: 12 August 2006

Abstract In this paper an approach to the validation of transient numerical simulations of turbulent flows through the use of time resolved PIV data is presented and applied to the case of turbulent flow within a simplified model of printed circuit board (PCB) enclosure. The comparison between numerical and experimental data is not limited here to the time averaged fields, but transient flow structures are also addressed. With this purpose a set of conditionally sampled averages, or cluster averages, are obtained through a Fuzzy Clustering technique. Further, the time history of the flow is analyzed on the base of this set of cluster averages, yielding time sequence relations among them that simplify their interpretation in terms of flow dynamics. In this way, events of alternate vortex shedding have been identified in a selected portion of the flow, and showed to exist in both numerical and experimental sets of data.

Key words conditional sampling · fuzzy clustering · vortex shedding

Supported by FPI/DPI2003-06725-C02-01 from DGI, Ministerio de Educación y Cultura y Fondos FEDER, and grant S/B/CE/33/07 from PDT Uruguay.

G. Usera
IMFIA, Universidad de la República, J.H. Reissig 565, 11300 Montevideo, Uruguay
e-mail: gusera@fing.edu.uy

A. Vernet · J. A. Ferré (✉)
Departament d'Enginyeria Mecánica, Universitat Rovira i Virgili, Av. Paisos Catalans 26, 43007 Tarragona, Spain
e-mail: josep.a.ferre@urv.net

A. Vernet
e-mail: anton.vernet@urv.net

1. Introduction

The overall aim of the ongoing research is to investigate the velocity field in complex domains and its influence on the heat transport by natural and/or forced convection. The specific application target is the turbulent flow and heat transport within printed circuit boards (PCB) enclosures. In the present stage of the investigation only the velocity field is under study, while plans for simultaneous measurement of velocity and temperature, through two-color Laser Induced Fluorescence (LIF) [8], are being implemented. In this paper experimental measurements obtained with time resolved PIV and numerical results from DNS at moderate Reynolds number will be analyzed and compared, with an emphasis on the transient behavior of the flow.

The increasing availability of full field measurement techniques with good time resolution (e.g. time resolved PIV) and of higher order numerical simulation methods for turbulent flows, (e.g. LES or DNS) provides the fluid dynamic researcher with databases of increased level of flow detail in the form of extended time series. To efficiently use these types of data, specialized methods need to be developed. Moreover, the validation of numerical simulation methods against time resolved PIV also requires methods that allow to check the transient dynamics of the simulation rather than just the mean statistical properties. Some of the widely used techniques that can be found in the literature are, among others, the Proper Orthogonal Decomposition (POD), the Pattern recognition (PR), and, to a lesser extent, the Singular Spectral Analysis (SSA), the Coherent Vortex Simulation (CVS), and Fuzzy Clustering (FC).

Proper orthogonal decomposition (POD) involves the computation of a subset of the eigenvectors and eigenvalues of the correlation tensor, in decreasing order of the eigenvalues magnitude. The eigenvectors with the largest eigenvalues can give an insight into the underlying large-scale structure of the flow [15]. The use of these leading eigenvectors as starting templates for pattern recognition in the search of coherent structures has been considered by [10]. In addition, the projection of the original data set onto the subset of eigenvectors, allows for reducing the dimensionality of the data set with a loss of information limited to the finer, and thus less energetic, scales of the flow. This is actually the purpose of applying POD within this work. A summary of the applications of the POD technique can be found in [1]. More recently, extensions based on POD have been proposed by [6, 13].

While POD is typically applied in the spatial domain, a class of techniques exist, named generically Singular Spectral Analysis, which extend the application of the POD concept to the time domain [7]. Multivariate SSA allows for simultaneous decompositions of the spatial and temporal domains into data adapted basis functions. Wavelet based orthogonal decomposition techniques have also been proposed, as for instance the (CVS) in [2, 3] as alternatives to POD. The Coherent Wavelet Simulation is a non-linear wavelet-based decomposition technique that adapts the number and selection of resolved modes, and keeps only the strongest wavelet coefficients at each time step. It thus rivals POD, which is a strategy with a fixed number of resolved modes, in terms of compression efficiency, although scarifying simplicity.

Pattern recognition comprises another set of techniques used to identify flow structures governing the dynamics of the flow [4, 5]. In PR prototypical structures or templates are correlated against instantaneous events to form ensemble averages, through an iterative procedure. However, usually only a moderate percentage of the instantaneous frames contained in the time series is involved in the pattern classification [10, 19].

On the other hand, fuzzy clustering is a technique that allows the classification of all the instantaneous frames into a specified number of conditionally averaged or coherent subsets [20]. This technique can identify flow structures whose existence remains hidden within the usual unconditional averaging procedure [18].

In this paper a novel conditional sampling method based on a fuzzy clustering technique is applied to the analysis of the large-scale structures of the turbulent flow in an experimental model of a PCB enclosing. To overcome the limitations of the conventional (unconditional) time averaging, a set of conditionally sampled averages, or cluster averages, are obtained with an improved signal-to-noise ratio. Further, the time history of the flow is analyzed on the base of this set of cluster averages, yielding the time sequence relations among them that simplify and complement their interpretation in terms of flow dynamics. This approach is applied to the validation of numerical simulations of this flow against time resolved PIV measurements.

2. Experimental Setup and Technique

The specific application targeted is the turbulent flow and heat transport within PCB enclosures. With this purpose a simplified model of such enclosure was built in transparent Plexiglas to allow optical access for the PIV system. The model was run with water in a closed circuit. The water entering the model was gravity driven from an elevated deposit to minimize perturbations, with a pump downstream of the model driving the water back to the elevated deposit. Typical flow rates were in the $100 - 500\, l/h$ range with maximum attainable flow rate at about $2,300\, l/h$.

A sketch of the experimental model is shown in Figure 1. The entrance and outlet openings have square sections of side $h = 0.024m$. The upper and lower channels are $6h$ long by $3h$ wide, and of height h each. The central plate is only $5h$ long. Two sets of measurements at different locations were obtained, at Reynolds numbers of $Re = 1.16 \times 10^3$ and 5.79×10^3 relative to the entrance section, which correspond to mean velocities at this section of $Uo = 4.8 \times 10^{-2}$ and $2.4 \times 10^{-1} m/s$, respectively. In this paper only the results at the lower Reynolds number are presented, with an emphasis on the separation region near the lower channel entrance, as pictured by region (D) in Figure 1.

Time resolved PIV recordings were obtained using an 420 by 480 pixels Motion Scope PCI 1000 S digital camera capable running at 125 and 250 Hz sampling rates for 512 image strips. The size of each image strip was limited by the internal memory of

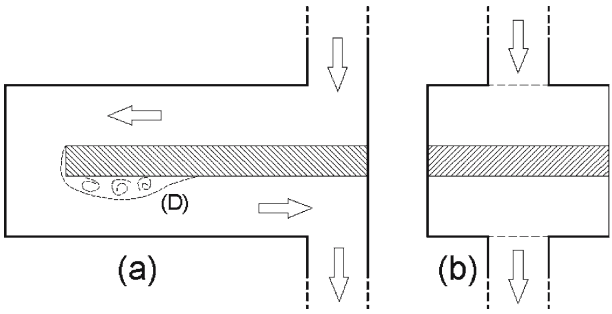

Figure 1 Sketch of experimental model with main paths of flow. **a** *Side view* with separation region (*D*) shown at the lower channel entrance. **b** *Front view*.

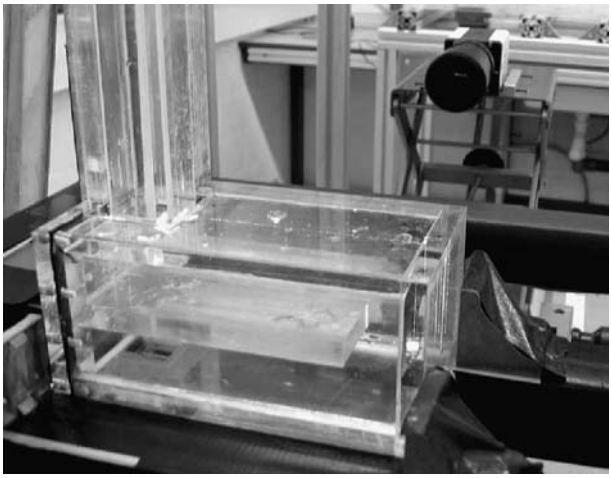

Figure 2 Image of experimental setup.

the camera. For the results presented here, at the lower Reynolds number, the lower sampling frequency was used. Illumination was provided by a Monocrom DPSSL 532 nm pulsed laser source, with a cylindrical lens. *Licopode* spores were used as seeding material, which absorb water providing almost spherical, neutrally buoyant, particles. An image of the experimental setup is presented in Figure 2 showing the Plexiglas model in the front and the PIV camera at the back. The Laser source is located to the right of the enclosure model, and reflections from the Laser beam onto the Plexiglas can be hinted at the outer shell of the model and at the front face of the inner plate.

The PIV processing algorithm used here is of the iterative pattern deformation type, following roughly the ideas of [14], and is described in detail in [17]. The iterative pattern deformation procedure allows for a spatial resolution that is almost independent of PIV interrogation area sizes and an enhanced behavior in strong gradient situations. Special care has been taken to improve the performance of the PIV interrogation near the wall boundaries, as well as to exploit the special characteristics of time resolved PIV recordings.

The time step between consecutive images is more than one order of magnitude smaller than representative integral time scales of the flow, as reported later in Section 5 and evidenced in Figure 9. Thus, the PIV recordings obtained in these experiments can be considered to be 'time resolved' in the sense discussed in [17]. A significant correlation will then exist between velocity fields obtained from consecutive pairs of images. This enables the application of multiple image correlation techniques together with reflection removal procedures to enhance the PIV processing [17]. The analysis of transient structures presented later also requires such degree of correlation between consecutive velocity fields.

3. Numerical Method

The numerical simulations considered here were obtained with the in-house flow solver *caffa3d.MB* developed at Rovira i Virgili University. It is an original Fortran95

implementation of a fully implicit finite volume method for solving the 3D incompressible Navier–Stokes equations in complex geometry. This three-dimensional solver is based on a two-dimensional solver described in [12].

Spatial discretization is based on block-structured, non-orthogonal, body fitted, collocated grids with first order (UDS) and second order (CDS) schemes for the convective terms. Improved linear interpolation schemes for non-orthogonal grids are also included following [11]. For the time discretization fully implicit two-level first order (implicit backward Euler) and three-level second order schemes are available. The SIMPLE algorithm is implemented for the coupling between velocity and pressure. Different interfaces between grid blocks are currently supported, among which only *one-to-one* interfaces are used in here. Domain decomposition on the basis of grid blocks is applied through OpenMP, with current simulation running on dual processor machines. A full description of the flow solver can be found in [16].

The grid for the current case was made of five regular blocks of resolution $h/40$, as pictured in Figure 3, for a total of 3.02×10^6 cells. Inlet and outlet duct blocks were used to minimize the effect of boundary conditions onto the region of interest of the flow. The dimensionless time step was $dt/(h/U_0) = 1 \times 10^{-2}$ and the simulation was allowed to reach a steady regime before collecting time series of results. Reynolds number was set to $Re = 1.16 \times 10^3$ as for experiments, and no turbulence model was applied.

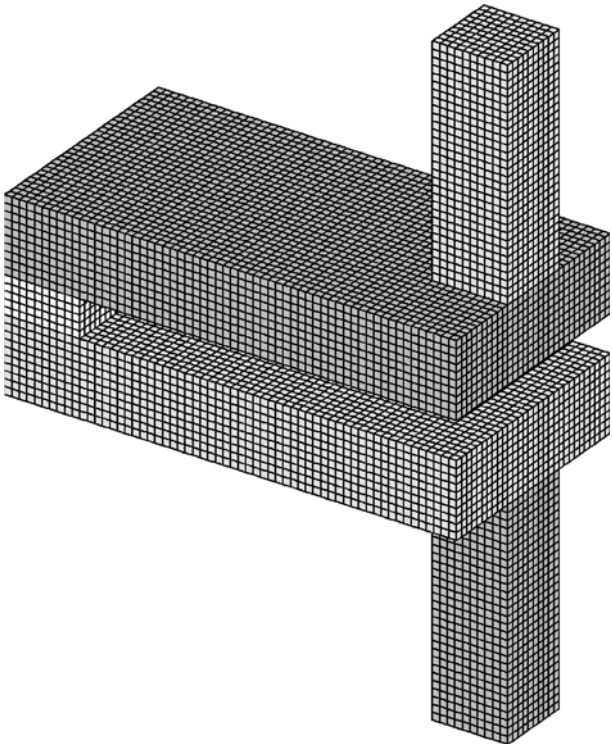

Figure 3 Numerical grid composed of five *matching* grid-blocks. Shown at $h/10$ resolution.

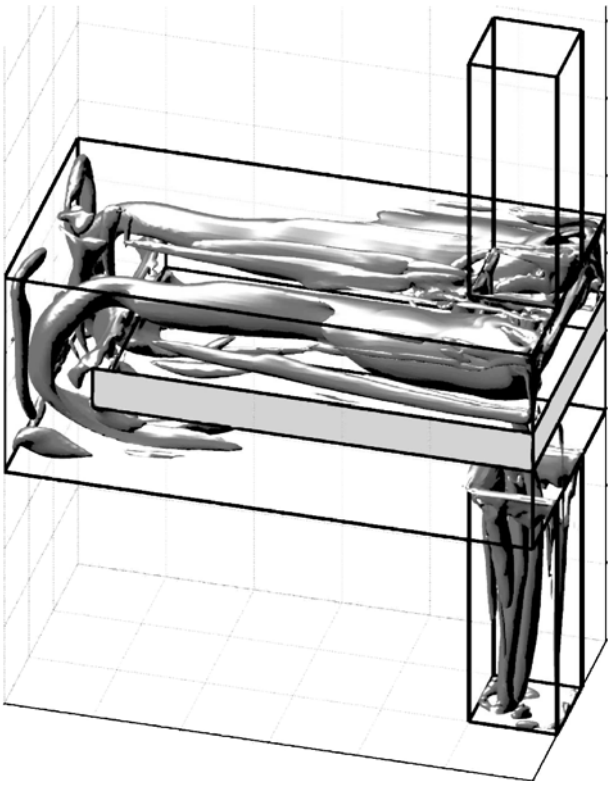

Figure 4 Vortical structures educed by λ_2 iso-surfaces from numerical simulation.

Figure 4 shows instantaneous vortical structures visualized by means of λ_2 iso-surfaces [9] obtained in the numerical simulation, in order to have an overview of the characteristics of the analyzed system. It can be seen that the flow in the upper channel is dominated by two counter rotating vortical structures. The non-stationary characteristic of the flow is also apparent from Figure 4.

4. Analysis of Mean Fields

The following analysis will be restricted to a portion of the flow, selected due to the interesting characteristics that the flow exhibits there and also because its expected role in the transport of heat away from the central plate, where the PCB would be located. The selected portion is the entrance to the lower channel in the vicinity of region (D) in Figure 1, beneath the central plate. Figure 5 shows the streamlines for the mean velocity field obtained from the ensemble averaged velocity field of the complete 2,550 frames PIV data set. Each PIV velocity field for the considered region contains $22 \times 64 = 1,408$ velocity vectors. It is seen that the mean velocity field is characterized, in the analyzed region, by a strong recirculation downstream from the leading edge of the plate, that separates the upper channel from the lower one, with the center of the re-circulation vortex at $x/h = 1.7$ and $y/h = 0.8$. Thus,

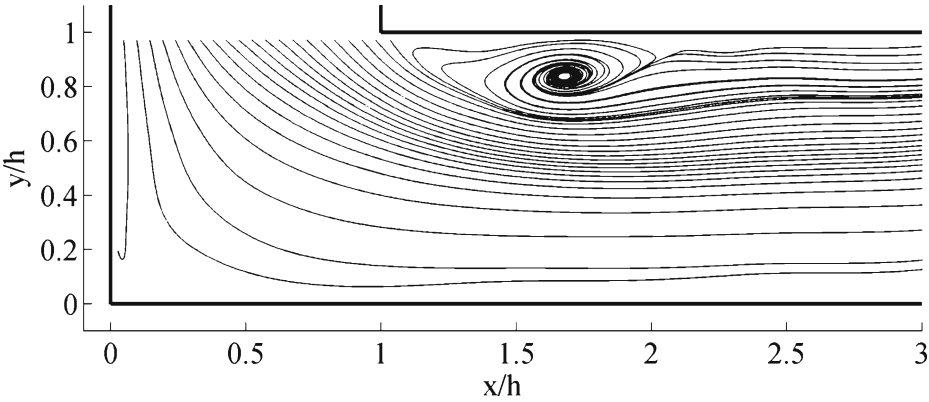

Figure 5 Mean velocity field streamlines in lower channel entrance region, showing re-circulation. Time resolved PIV experimental results.

the main flow entering the lower channel is deflected downwards, passing through a section of height about 2/3 of the total height of the channel.

This type of representation of the mean flow should not be pushed too far in drawing conclusions about the dynamics of the flow. For instance, if the instantaneous flow was to be permanently as pictured in Figure 5, the heat transfer from the plate near the re-circulation region could be adversely affected. This would be so because little exchange with the main flow entering the lower channel would be allowed. Thus, it is important to assess the transient evolution of the flow in this region, since transport of heat away from the plate might be enhanced by transient structures.

The reminder of this analysis will be based onto the spanwise vorticity field, since it is expected to be well suited to reveal the underlying structures in the re-circulation

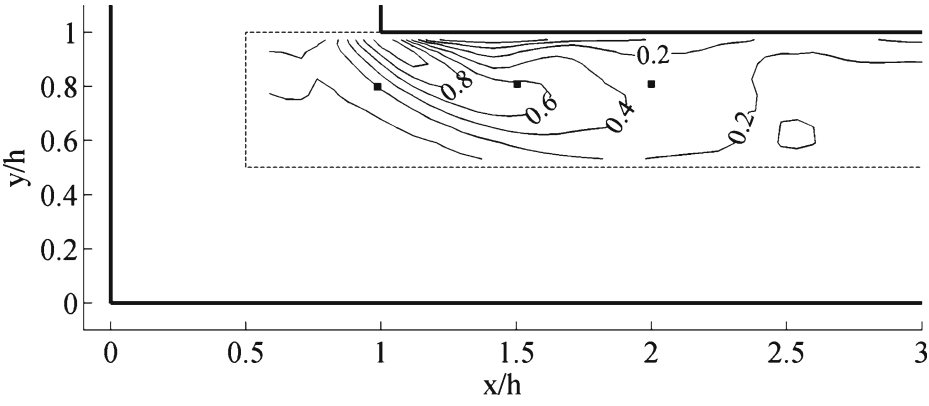

Figure 6 Normalized mean spanwise vorticity contours ($\omega_z/(2U_0/h)$). Time resolved PIV experimental results.

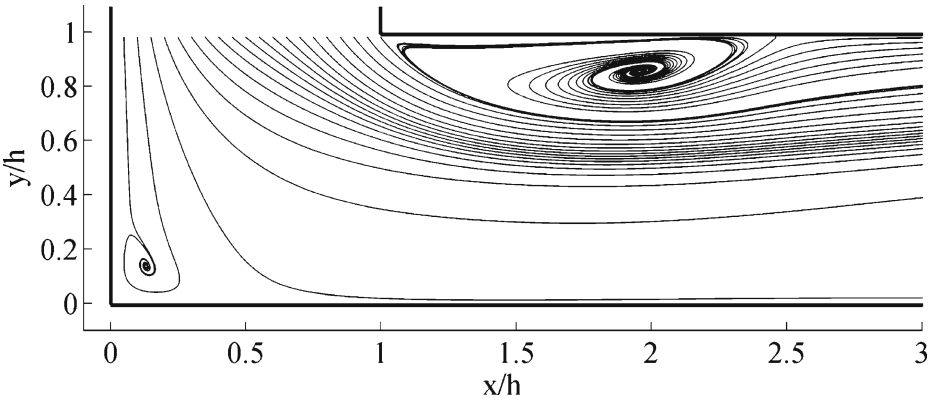

Figure 7 Mean velocity field streamlines in lower channel entrance region. Numerical simulation results.

region, which are expected to be mainly vortical structures. In Figure 6, the mean dimensionless spanwise vorticity field is pictured, as defined by:

$$\omega_z \cdot \frac{h}{2U_0} = \left(\frac{\partial v}{\partial x} - \frac{\partial u}{\partial y}\right) \cdot \frac{h}{2U_0} \tag{1}$$

where U_0 is the main velocity relative to the entrance section, u and v are the streamwise and vertical velocity components, and $h/2$ is the half height of the channel.

Figure 6 shows that the relative maximum of vorticity is roughly aligned with the shear layer defined between the main flow entering the lower channel and the re-circulation area. This layer weakens towards $x/h = 2.5$ marking the downstream extension of the re-circulation area. A region of interest around the re-circulation area has been marked with a dashed line in Figure 6. Further plots will be restricted only to this region of interest.

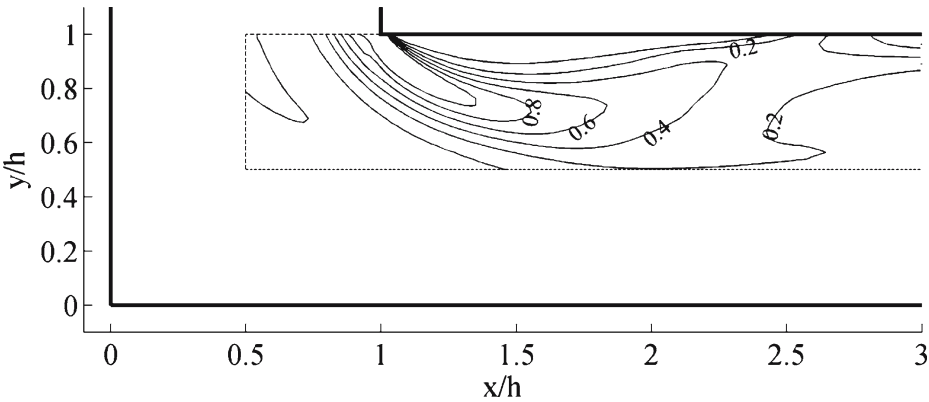

Figure 8 Normalized mean spanwise vorticity contours ($\omega_z/(2U_0/h)$). Numerical simulation results.

These results for the mean flow obtained from the PIV experimental measurements will be compared now with corresponding results from the numerical simulation, obtained after averaging over 1.3×10^2 integral time scales of the flow. Figure 7 presents mean flow streamlines while in Figure 8 mean normalized spanwise vorticity contours are given, corresponding, respectively, to Figures 5 and 6.

The patterns of streamlines pictured in Figures 5 and 7 are quite similar. The vertical extension of the recirculation regions is approximately $h/3$ in both cases, with the center of the recirculation pattern slightly displaced downstream in the numerical simulation results respect to the PIV experimental results. Also a small vortex appears at the lower left corner in the numerical results that is hidden in the PIV results, probably due to their lower resolution.

Mean spanwise vorticity contours of Figures 6 and 8 exhibit an even better agreement. Contour levels match very closely, being slightly higher for the numerical results, again probably due to their higher resolution. Still, the downstream weakening of the shear layer near $x/h = 2.5$ is quite well reproduced.

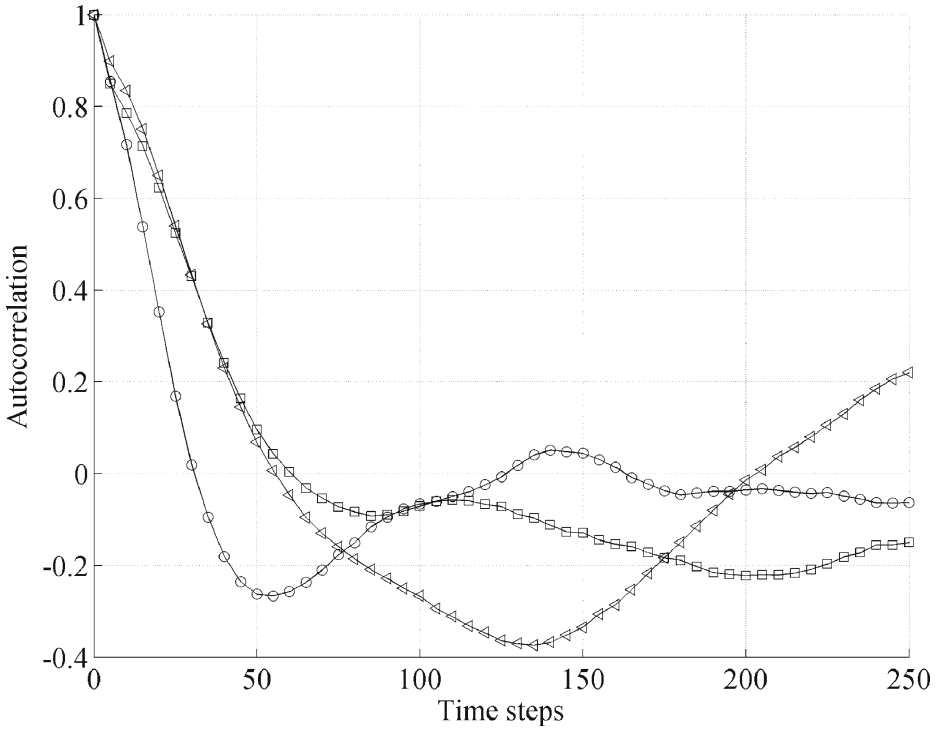

Figure 9 Auto-correlation of spanwise vorticity time series at $y/h = 0.8$ and $x/h = 1.0$ (-o-), $x/h = 1.5$ (-∇-) and $x/h = 2.0$ (-□-).

5. Analysis of Transient Structures

The analysis of the transient structures arising in the region marked in Figure 6 is considered next. This analysis will be first presented for the experimental data and then results from both experimental and numerical data sets will be compared. The analysis method followed here, combining POD and FC, was first described in [18].

First, the auto-correlation function for the spanwise vorticity time series was computed at selected locations, from the PIV data set. These auto-correlation

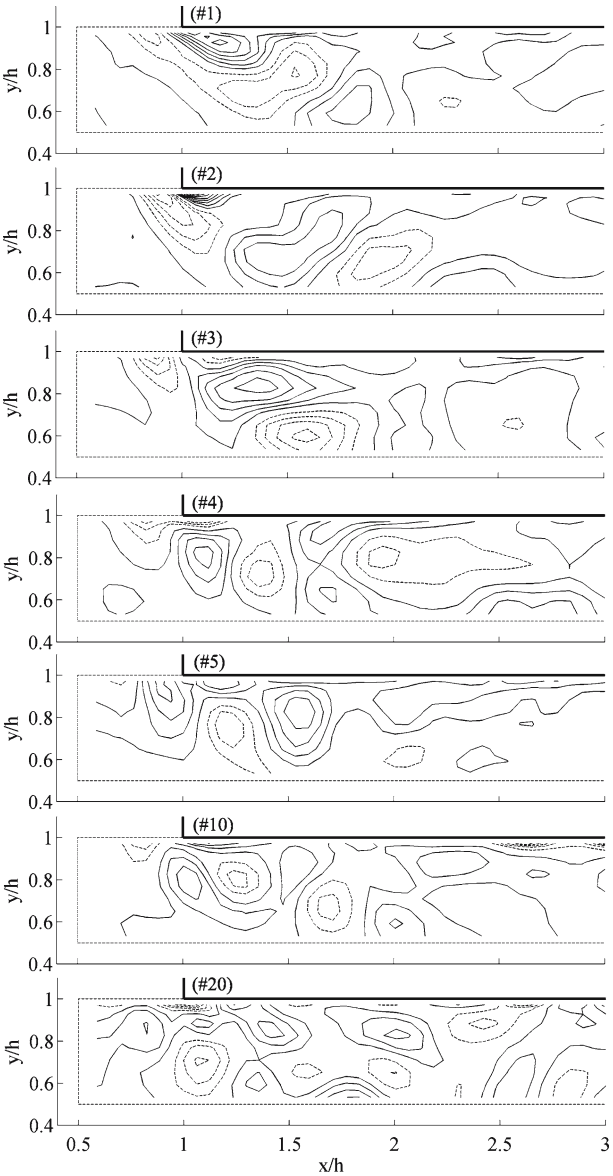

Figure 10 POD eigenvectors for spanwise vorticity field. From *top to bottom*: #1, #2, #3, #4, #5, #10, #20.

functions are plotted in Figure 9. The three selected locations are indicated in Figure 6 by small squares and their co-ordinates are $y/h = 0.8$ and $x/h = 1.0, 1.5, 2.0$. The first one falls in the main flow, right outside the re-circulation region, while the second and third lie within this region. Dimensionless integral time scales for vorticity fluctuations at these locations are $T/dt = 1.5 \times 10^1, 2.4 \times 10^1, 2.4 \times 10^1$, respectively, while the dimensionless sampling time for each PIV series was $Ts/dt = 510$. Thus, the whole PIV experimental time series spanned about 1.1×10^2 integral time scales.

In relation to Figure 9, it is worth noting that, while the auto-correlation functions at locations 1 and 3 oscillate around zero after a few integral time scales, in the case of location 2 the auto-correlation function exhibits a deeper oscillation of larger amplitude and duration. This might reveal the existence of cyclic vortex passing near this location, which in fact will be later confirmed by the clustering analysis below.

Next, proper orthogonal decomposition was applied to the time series of instantaneous spanwise vorticity fields within the dashed region of Figure 6, which consisted of $10 \times 48 = 480$ grid points and 2,550 time steps assembled in five series of 510 time steps each. The first 40 eigenvectors and eigenvalues were computed, accounting cumulatively for up to 70% of the total variance and with the last eigenvalue accounting for less than 1% of it. The *normalized* eigenvector vorticity fields for eigenvalues 1, 2, 3, 4, 5, 10 and 20 are given in Figure 10 that shows an increasingly

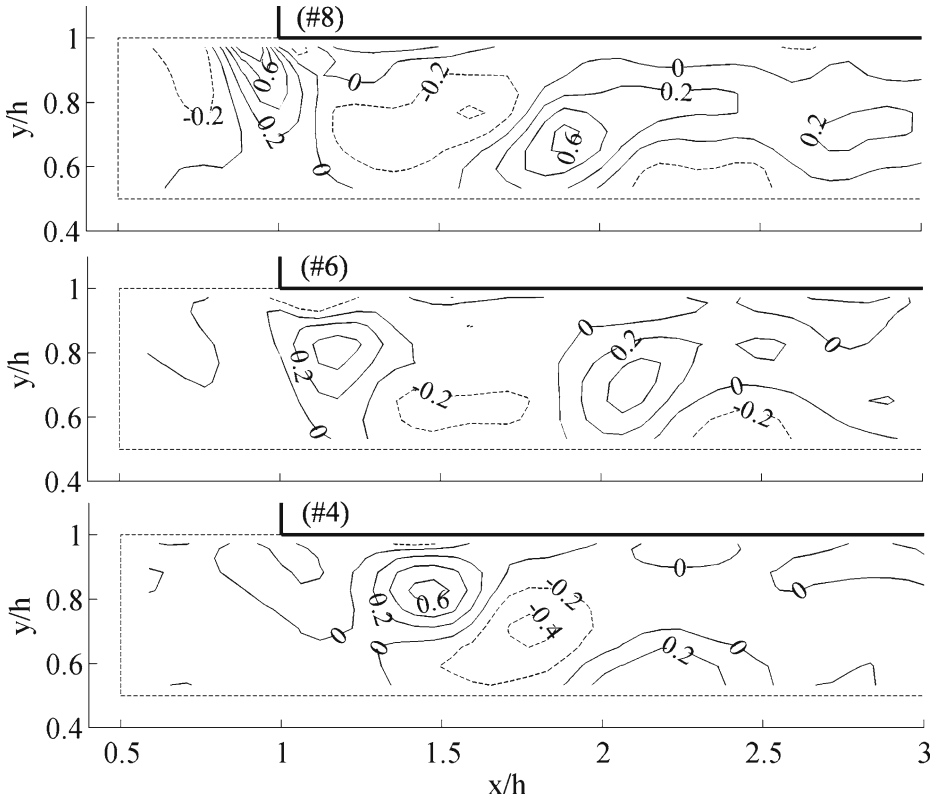

Figure 11 Cluster sequence #8-6-4. Time resolved PIV experimental results.

finer hierarchy of vortical structures, as expected from a spectral like decomposition, with alternate vorticity sign within the re-circulation region.

However, the analysis of the eigenvectors alone gives no indication of the temporal evolution of these structures. It should be noted that the results from POD analysis would be the same regardless of the temporal organization of the instantaneous time steps. The information regarding the temporal organization of the flow is kept then in the projections of the time series onto these eigenvalues and an analysis of these time series of projections is required in order to recover this information. This will be the objective of the following paragraphs where a fuzzy clustering algorithm will be first presented and then applied to determine a set of ensemble averages or clusters, which picture the most representative states of the flow and the transitions between them.

5.1. Fuzzy clustering algorithm

The fuzzy clustering algorithm applied here is the c-Means clustering algorithm coupled with a validity criteria proposed by Xie and Beni, both of which are described in a general context in [21]. Application of this method to time series of fields in fluid

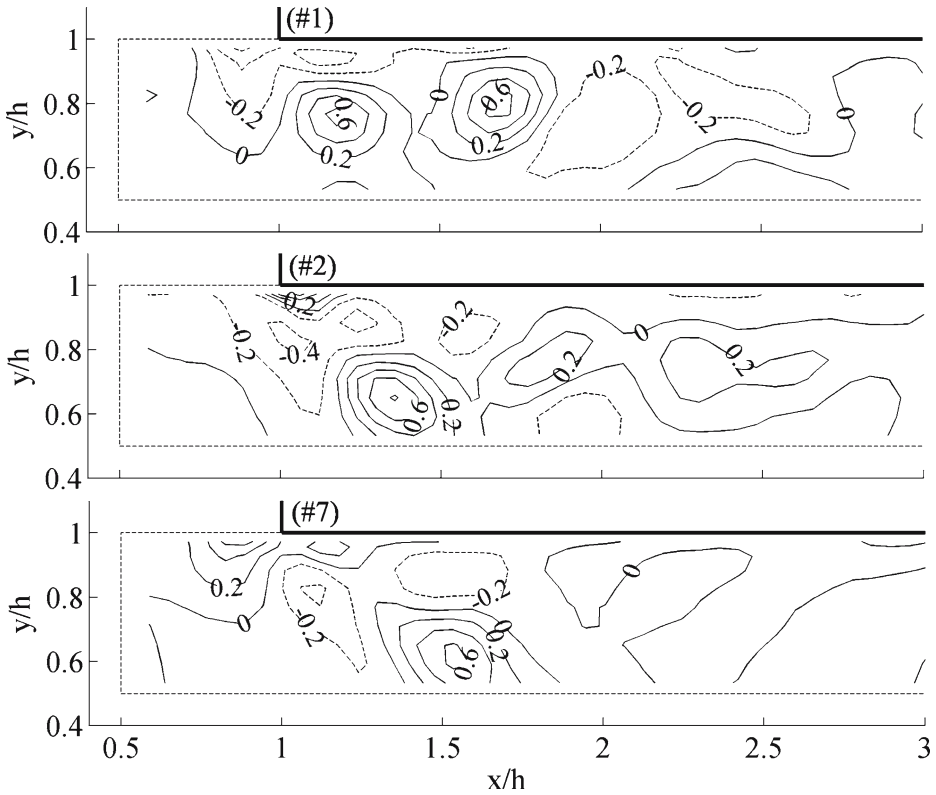

Figure 12 Cluster sequence #1-2-7. Time resolved PIV experimental results.

dynamics has been proposed in [18, 20]. Here a brief description of the method will be given following [21] and [18].

The c-Means Clustering Algorithm seeks the minimization, for a prescribed number of clusters c, and fuzziness index m ($m > 1$), of an objective function J_m, defined as:

$$J_m = \sum_{i=1}^{c} \sum_{j=1}^{n} \left(\mu_{ij}\right)^m d^2\left(X_j, V_i\right) \tag{2}$$

where X_j (j=1,2,...,n) is the data set to be clustered and $d^2(X_j, V_i)$ is a measure of the distance between the vectors X_j and the cluster center V_i, usually taken as the Euclidean distance, and μ_{ij} is the fuzzy membership function that verifies the condition:

$$\sum_{i=1}^{c} \mu_{ij} = 1 \tag{3}$$

For any partition, the cluster centroids are defined from:

$$V_i = \frac{\sum_{j=1}^{n} \left(\mu_{ij}\right)^m X_j}{\sum_{j=1}^{n} \left(\mu_{ij}\right)^m} \tag{4}$$

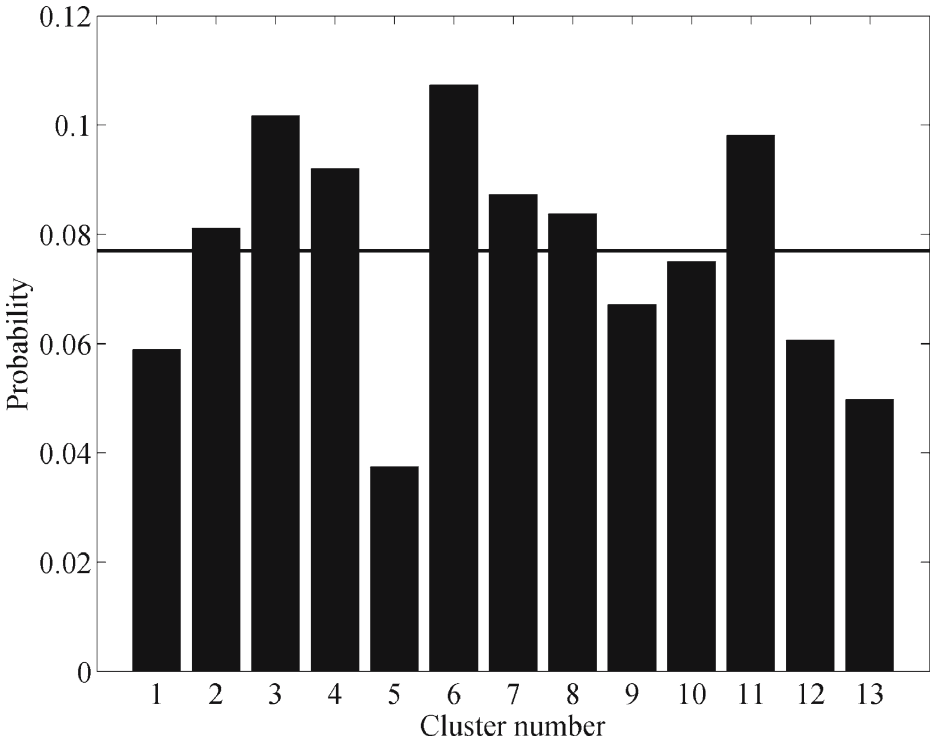

Figure 13 Probability of occurrence of each cluster. *Thick line* indicates the mean probability (1/13). Time resolved PIV experimental results.

Also, the fuzzy membership function can be computed from a specified set of centroids V_i from:

$$\mu_{ij} = \frac{\left(\frac{1}{d^2(X_j, V_i)}\right)^{\frac{1}{m-1}}}{\sum_{i=1}^{c}\left(\frac{1}{d^2(X_j, V_i)}\right)^{\frac{1}{m-1}}} \tag{5}$$

The minimization of J_m is attained by iterating equations (4) and (5) from a starting guess of either μ_{ij} or V_i until no further improvement of J_m (Equation (2)) is observed.

Still, the c-Means Clustering Algorithm by itself gives no clue about the number of clusters to be used in partitioning the set. In order to determine the optimum number of clusters to be used for each data set, as well as the value of the fuzziness index m, the validity criterion for fuzzy clustering [21], was applied. For any given partitioning, regardless of the algorithm used to determine it, a compactness and separation validity function S, can be defined as:

$$S = \frac{\sum_{i=1}^{c}\sum_{j=1}^{n}\mu_{ij}^2 d^2\left(X_j, V_i\right)}{n \cdot min_{ij} d^2\left(X_j, V_i\right)} \tag{6}$$

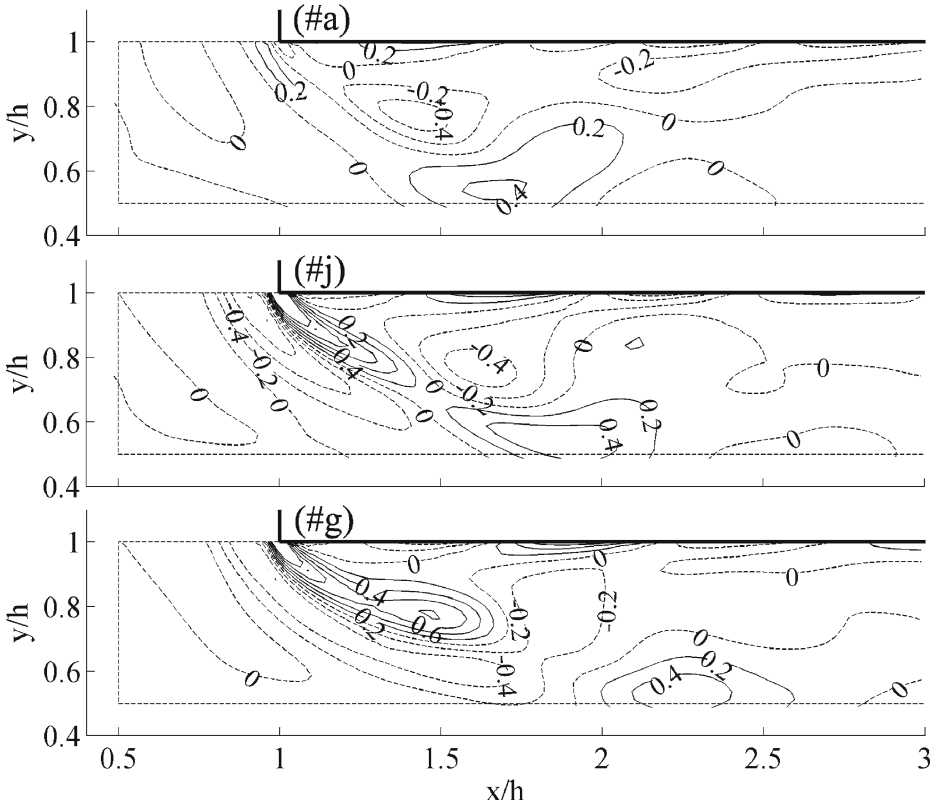

Figure 14 Cluster sequence #a-j-g. Numerical simulation results.

The validity function S can be regarded as the ratio of the measure of the compactness of the clusters over the minimum separation among clusters. Optimum values of c and m are those for which S reaches an absolute minimum value. In some cases however one might be content to find a relative minimum value.

5.2. Fuzzy clustering results

The FC algorithm described in the previous section, together with the partition validity criterion, was applied to the PIV data set. For the vorticity field data considered before an optimum value for S was found at $c = 13$ and $m = 1.16$. Not all cluster ensemble averages will be reproduced here, but only six of them selected due to the frequent transitions that the flow exhibits among them.

In Figure 11 a first set of three clusters, or ensemble averages for spanwise vorticity fluctuations, is presented comprising clusters #8, #6 and #4, while in Figure 12 the second set contains clusters #1, #2 and #7. The cluster index is assigned arbitrarily during the iteration process. The ordering of the clusters among each set was decided according to the sequence of the transitions of the flow between states corresponding to each cluster.

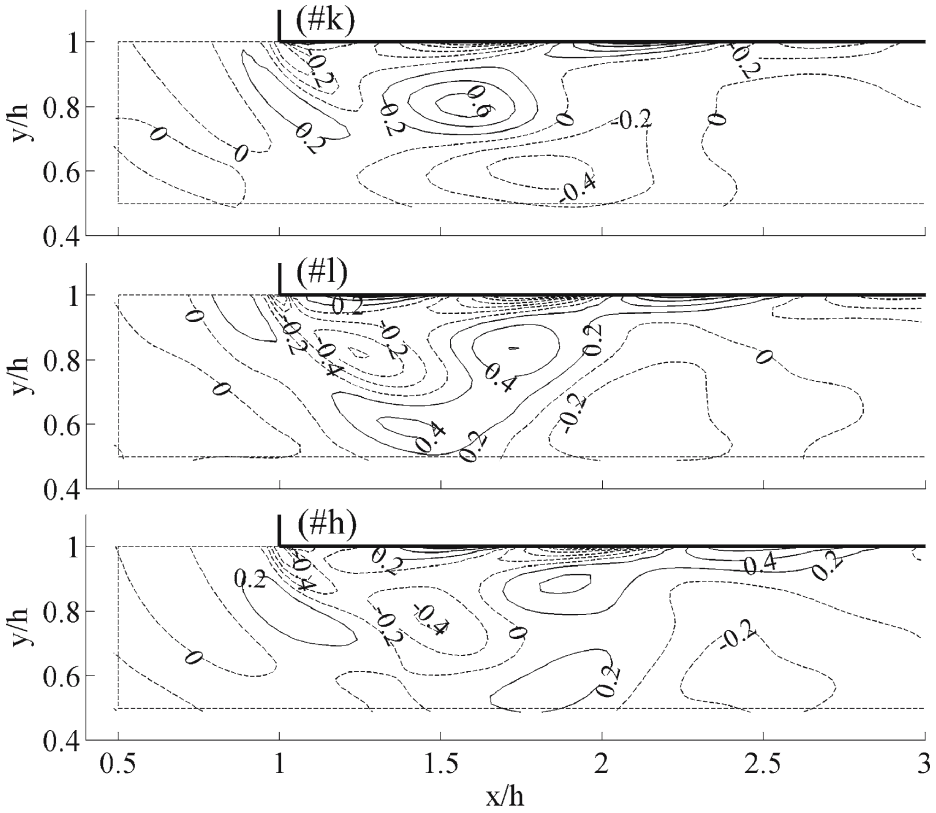

Figure 15 Cluster sequence #k-l-h. Numerical simulation results.

Figure 11 shows that an array of vorticity fluctuation spots with alternate sign evolve downstream. In particular a positive vorticity spot forms near the leading edge of the plate (clusters #8 and #6) and then drifts downstream (clusters #6 and #4). A similar picture emerges in Figure 12, although there the vortex forming at the leading edge has negative spanwise vorticity, while a vortex with positive spanwise vorticity is evolving downstream and away from the plate. The downstream drift of these structures is expected to be associated with a net transport of heat away from the plate that would enhance the limited transport of heat associated solely to the re-circulation pattern of the mean velocity field.

The probability of occurrence of each cluster is given in Figure 13. This figure can also be interpreted as the percentage of cumulative time spent by the flow in configurations classified as belonging to each cluster. From this point of view, the series presented in Figures 11 and 12 account, respectively, for 22% and 28% of the time, so that together they represent the evolution of the flow for about 50% of the total time.

Corresponding results obtained by applying the same FC procedure to the numerical simulation data set are presented now, for comparison with the experimental results. In this case, an optimum value for S was found at $c = 12$ and $m = 1.24$. While the near coincidence in the number of clusters found to be optimal for the classification is encouraging, it is most interesting to check whether the cluster ensemble

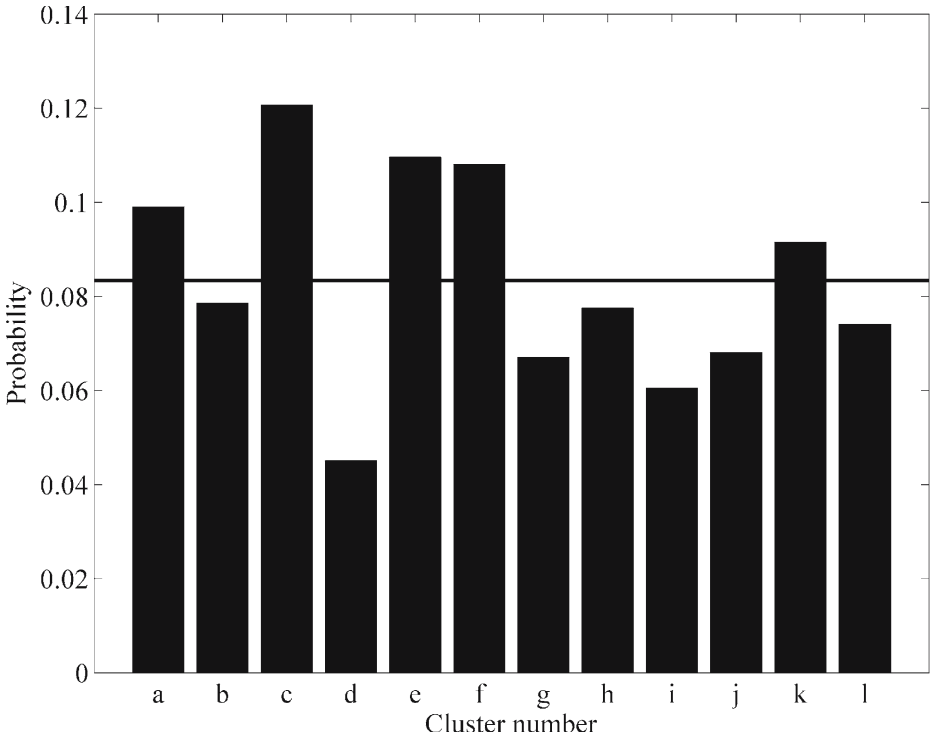

Figure 16 Probability of occurrence of each cluster. *Thick line* indicates the mean probability (1/12). Numerical simulation results.

averages themselves depict similar patterns as those found for the experimental data set.

Again two sequences of three clusters were selected, based on the frequent transitions between them observed in the flow. Since the initial indexing of clusters is arbitrary, letters have been assigned to the clusters obtained from the numerical data set to prevent confusion with the experimental ones. Thus, Figure 14 presents the cluster ensemble average sequence #a-j-g of spanwise vorticity fluctuation contours, while in Figure 15 sequence #k-l-h is presented. The selected cluster ensembles amount for up to 48% of the total time of simulated flow time series, as can be seen from Figure 16.

The evolution of vortical structures in Figures 14 and 15 resembles that of Figures 11 and 12, evidencing that the numerical simulation is in fact reproducing the same vortex shedding dynamics observed in the experimental results. The comparison between sequences is not necessarily on the basis of individual cluster ensembles, but rather on the trend expressed by the cluster ensemble sequences.

Figures 11, 12, 14 and 15 presented cluster ensemble averages of spanwise vorticity fluctuations. A complementary view can be given by adding the mean spanwise vorticity field to the spanwise vorticity fluctuations. This is pictured in Figure 17 for

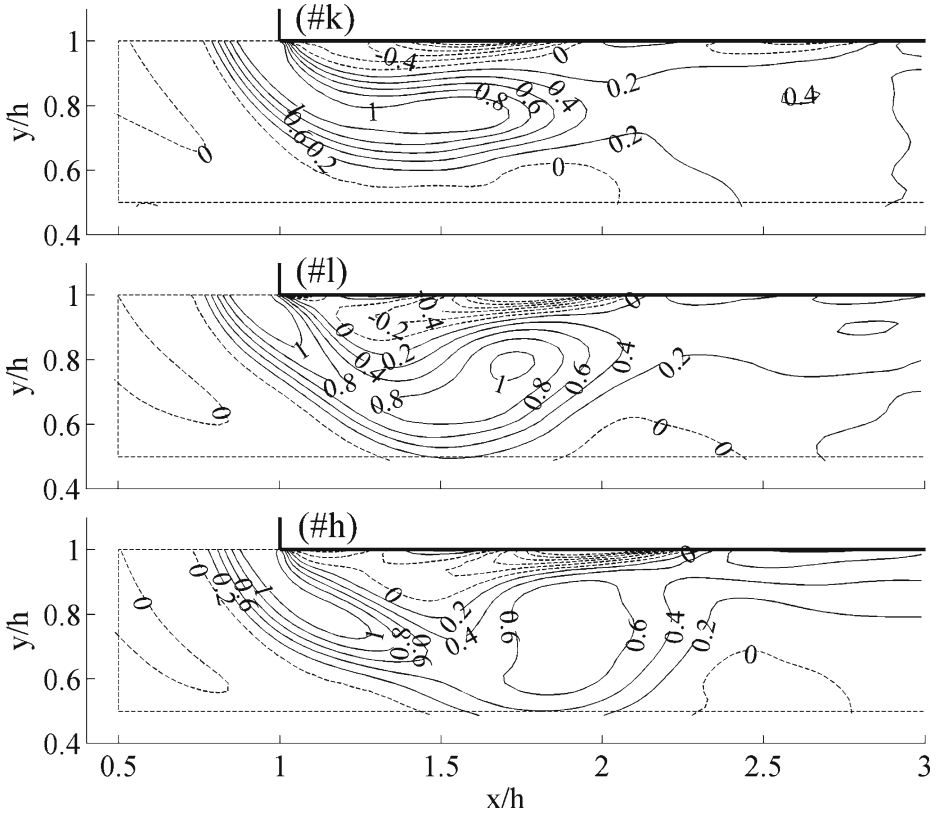

Figure 17 Cluster sequence #k-l-h, superimposed to the mean field. Numerical simulation results.

the case of cluster sequence #k-l-h obtained from the numerical data set. Vorticity contours in Figure 17 show a flapping shear layer that sheds a vortex, which then drifts downstream.

6. Conclusions

The flow within a simplified model of a printed circuit board (PCB) enclosing has been analyzed both experimentally and numerically, focusing on a selected portion of the flow.

A conditional sampling technique based on a Fuzzy Clustering algorithm has been applied to the analysis of time series of spanwise vorticity fields obtained from time resolved PIV and from the transient numerical simulations. This procedure allows for the comparison of not only mean average fields, but also of sequences of conditionally sampled ensemble averages. In this way validation of the numerical simulation against the experiments is not limited to the mean statistical properties of the flow, so that the transient behavior of the flow can be compared too.

The selected portion of the flow presented in this communication shows a recirculation region beneath the plate at the entrance of the lower channel. Events of alternate vortex shedding have been identified through the fuzzy clustering analysis, in both experimental and numerical data sets. These events, which were hinted by the auto-correlation function, may enhance the transport of heat beneath the plate, with respect to that which would be produced by the mean flow.

Future work will consider an evaluation of the temperature field and its relationship with the velocity through simultaneous measurements with two-color Laser Induced Fluorescence (LIF) in order to quantify the effect of these structures on the transport of heat.

References

1. Berkooz, G., Holmes, P., Lumeley, J.L.: The proper orthogonal decomposition in the analysis of turbulent flows. Annu. Rev. Fluid Mech. **25**, 539–575 (1993)
2. Farge, M., Schneider, K.: Coherent Vortex Simulation (CVS), a semi-deterministic turbulence model using wavelets. Flow Turbul. Combust. **66**, 393–426 (2001)
3. Farge, M., Schneider, K., Pellegrino, G., Wray, A.A., Rogallo, R.S.: Coherent vortex extraction in three-dimensional homogeneous turbulence: Comparison between CVS-wavelet and POD–Fourier decompositions. Phys. Fluids **15**(10), 2886–2896 (2003)
4. Ferré, J.A., Giralt, F.: Pattern-recognition analysis of the velocity field in plane turbulent wakes. J. Fluid Mech. **198**, 27–64 (1989)
5. Ferré, J.A., Mumford, J.C., Savill, A.M., Giralt, F.: Three-dimensional large eddy motions and fine-scale activity in a plane turbulent wake. J. Fluid Mech. **210**, 371–414 (1990)
6. Garnard, S., George, W.K., Jung, D., Woodwrad, S.: Application of a *slice* proper orthogonal decomposition to the far field of an axisymmetric turbulent jet. Phys. Fluids **14**(7), 2515–2522 (2002)
7. Ghil, M., Allen, M.R., Dettinger, M.D., Ide, K., Kondrashov, D., Mann, M.E., Robertson, A.W., Saunders, A., Tian, Y., Varadi, F., Yiou, P.: Advanced spectral methods for climatic time series. Rev. Geophys. **40**, 1 (2002)
8. Hishida, K., Sakakibara, J.: Combined planar laser-induced fluorescence-particle image velocimetry technique for velocity and temperature fields. Exp. Fluids **29**, 129–140 (2000)
9. Jeong, J., Hussain, F.: On the identification of a vortex. J. Fluid Mech. **285**, 69–94 (1995)

10. Kopp, G.A., Ferré, J.A., Giralt, F.: The use of pattern recognition and proper orthogonal decomposition in identifying the structure of fully-developed free turbulence. J. Fluids Eng. **119**, 289–296 (1997)
11. Lehnhauser, T., Schafer, M.: Improved linear interpolation practice for finite-volume schemes on complex grids. Int. J. Numer. Methods Fluids **38**, 625–645 (2002)
12. Lilek, Z., Muzaferija, S., Peric, M., Seidl, V.: An implicit finite-volume method using nonmatching blocks of structured grid. Numer. Heat Transf., Part B **32**, 385–401 (1997)
13. Maurel, S., Borée, J., Lumley, J.L.: Extended proper orthogonal decomposition: Application to Jet/Vortex interaction. Flow Turbul. Combust. **67**, 125–136 (2001)
14. Nogueira, J., Lecuona, A., Rodríguez, P.A.: Local field correction PIV, implemented by means of simple algorithms and multigrid versions. Meas. Sci. Technol. **12**, 1911–1921 (2001)
15. Reichert, R.S., Hatay, F.F., Biringen, S., Huser, A.: Proper orthogonal decomposition applied to turbulent flow in a square duct. Phys. Fluids **6**(9), 3086–3092 (1994)
16. Usera, G., Vernet, A., Ferré, J.A.: Simulación numérica de las ecuaciones de Navier Stokes en 3D, por volúmenes finitos en mallas curvilíneas estructuradas por bloques. Congreso de Métodos Numéricos en Ingeniería, Granada, Spain (2005)
17. Usera, G., Vernet, A., Ferré, J.A.: Considerations and improvements on analyzing algorithms for time resolved PIV of turbulent wall bounded flows. In: 12th International Symposium. Applications of Laser Techniques to Fluid Mechanics (2004)
18. Usera, G., Vernet, A., Pallares, J., Ferré, J.A.: A conditional sampling method based on fuzzy clustering for the analysis of large-scale dynamics in turbulent flows. Eur. J. Mech. B, Fluids **25**(2), 172–191 (2006)
19. Vernet, A., Kopp, G.A., Ferré, J.A., Giralt, F.: Three-dimensional structure and momentum transfer in a turbulent cylinder wake. J. Fluid Mech. **394**, 303–337 (1999)
20. Vernet, A., Kopp, G.A.: Classification of turbulent flow patterns with fuzzy clustering. Eng. Appl. Artif. Intell. **15**(3–4), 315–326 (2002)
21. Xie, X.L., Beni, G.: A validity measure for fuzzy clustering. IEEE Trans. Pattern Anal. Mach. Intell. **PAMI-13**(8), 841–847 (1991)